EPR Spectroscopy of Radical Ions of a 2,3-Diamino-1,4-naphthoquinone Derivative

Ján Tarábek,[§] Jin Wen,[§] Paul I. Dron,[†] Lubomír Pospíšil,[§,¶] and Josef Michl[§,†*]

[§] Institute of Organic Chemistry and Biochemistry, Flemingovo nám. 2, 16610 Prague, Czech Republic

[†] Department of Chemistry and Biochemistry, University of Colorado, Boulder, CO 80309-0215, U.S.A.

[¶] J. Heyrovský Institute of Physical Chemistry, Dolejškova 3, 18223 Prague, Czech Republic

Table of Contents Graphic

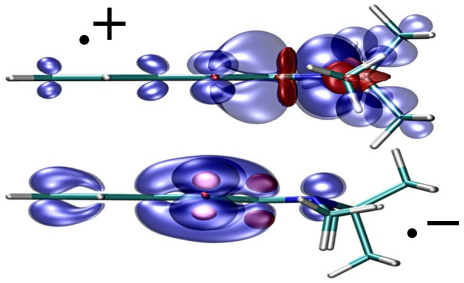

Abstract

We report the electron paramagnetic resonance spectra of the radical cation and radical anion of 1,2,2,3-tetramethyl-2,3-dihydro-1H-naphtho[2,3-d]imidazole-4,9-dione (**1**) and its doubly ^{13}C labeled analog **2**, of interest for singlet fission. The hyperfine coupling constants are in excellent

agreement with density functional theory calculations and establish the structures beyond doubt. Unlike the radical cation $\mathbf{1}^{\bullet+}$, the radical anion $\mathbf{1}^{\bullet-}$ and its parent **1** have pyramidalized nitrogen atoms and inequivalent methyl groups 15 and 16, in agreement with the calculations. The distinction is particularly clear with the labeled analog $\mathbf{2}^{\bullet-}$.

Introduction

Quantum chemical calculations suggest that captodatively substituted biradicals and biradicaloids are likely candidates for having similar S_0-T_1 and T_1-S_1 gaps and thus are of potential interest for studies of singlet fission.[1] Singlet fission is a process that generates two triplet excitons from one singlet exciton and a ground-state molecule[2] and promises a considerable increase in the efficiency of inexpensive solar cells.[3,4] At present, it suffers from a paucity of suitable materials, and many laboratories pursue searches of new suitable structures.

1,4-Quinones with donor groups in 2- and 3-positions can be viewed as captodatively substituted biradicaloids. They represent a surprisingly little known class of compounds and would seem worthy of an examination. EPR studies of their radical ions are even rarer and we have found none of radical cations. We have also failed to find any reported spectra of radical anions with two amino groups in the critical 2- and 3-positions of 1,4-naphthoquinone, and only two with a single amino group.[5,6] One of the few known simple derivatives of 2,3-diamino-1,4-naphthoquinone is 1,2,2,3-tetramethyl-2,3-dihydro-1H-naphtho[2,3-*d*]imidazole-4,9-dione[7] (**1**). Its photophysical behavior can be expected to be simplified relative to that of the parent, since proton translocation and extensive C-N bond twisting are prevented, and it is currently under investigation in our laboratory.

Intermolecular charge-transfer events are important in studies of singlet fission. On the one hand, they may promote the process, and on the other, they may introduce undesired transients and deactivation pathways. In parallel to improving the synthesis and characterization of **1** and examining its photophysical behavior, we have therefore also investigated its electrochemical reduction and oxidation and found that both processes are reversible.[8] One-electron oxidation of **1** occurs at $E_{1/2}^{ox} = +0.447$ V, the first one-electron reduction at $E_{1/2}^{red1} = -0.840$ V, and the second one-electron reduction at $E_{1/2}^{red2} = -1.445$ V, all relative to Ag/AgCl. The second reduction is expected to yield a closed-shell species devoid of EPR signals, but the two one-electron processes should yield the EPR-active radical cation $\mathbf{1}^{\bullet+}$ and radical anion $\mathbf{1}^{\bullet-}$, respectively. We reported their UV-visible absorption spectra, but did not provide a rigorous structure proof. In the present paper, we record and analyze the electron paramagnetic resonance (EPR) spectra of the two ions, which yield hyperfine coupling constants in excellent agreement with density functional theory (DFT) calculations and establish their structure beyond doubt. It is interesting that unlike the radical cation $\mathbf{1}^{\bullet+}$, the radical anion $\mathbf{1}^{\bullet-}$ and its parent **1** have pyramidalized nitrogen atoms and inequivalent methyl groups 15 and 16, in agreement with the DFT calculations.

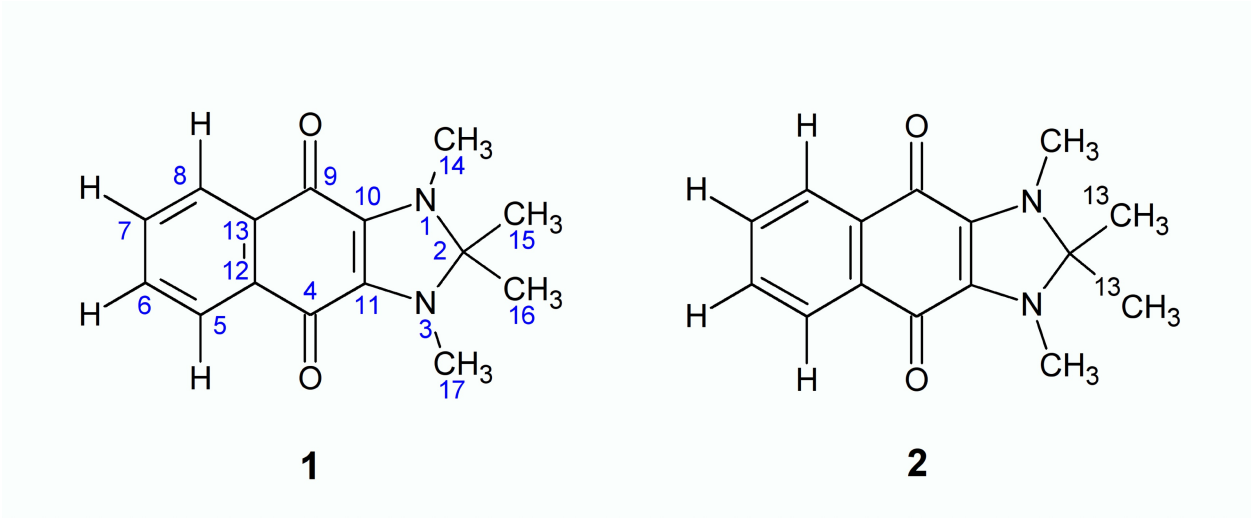

Figure 1. Structure of 1,2,2,3-tetramethyl-2,3-dihydro-1H-naphtho[2,3-d]imidazole-4,9-dione (**1**) and its ^{13}C-labeled derivative (**2**). Atom numbering is the same for both structures.

Results

The spectra obtained in $CH_3CN/TBAPF_6$ and in $DMSO/TBAPF_6$ were similar. We focus on the latter since they were better resolved (Supporting Information) and provided access to higher temperatures. Both radical ions were relatively persistent at room temperature and their spectra could be recorded for at least 40 min after their potentiostatic generation at the first oxidation/reduction peak potential (cf. Figure S5 in the Supporting Information).

Radical Cation 1$^{\bullet+}$. The hyperfine coupling/splitting constants deduced from the simulation of the EPR spectrum shown in Figure 2 are collected in Table 1 together with their DFT-calculated counterparts. The agreement is excellent, with the largest discrepancy of 3.42 MHz/0.12 mT, and we consider the structure confirmed. We have not found data for any radical cations of similar donor-substituted 1,4-naphthoquinones in the literature.

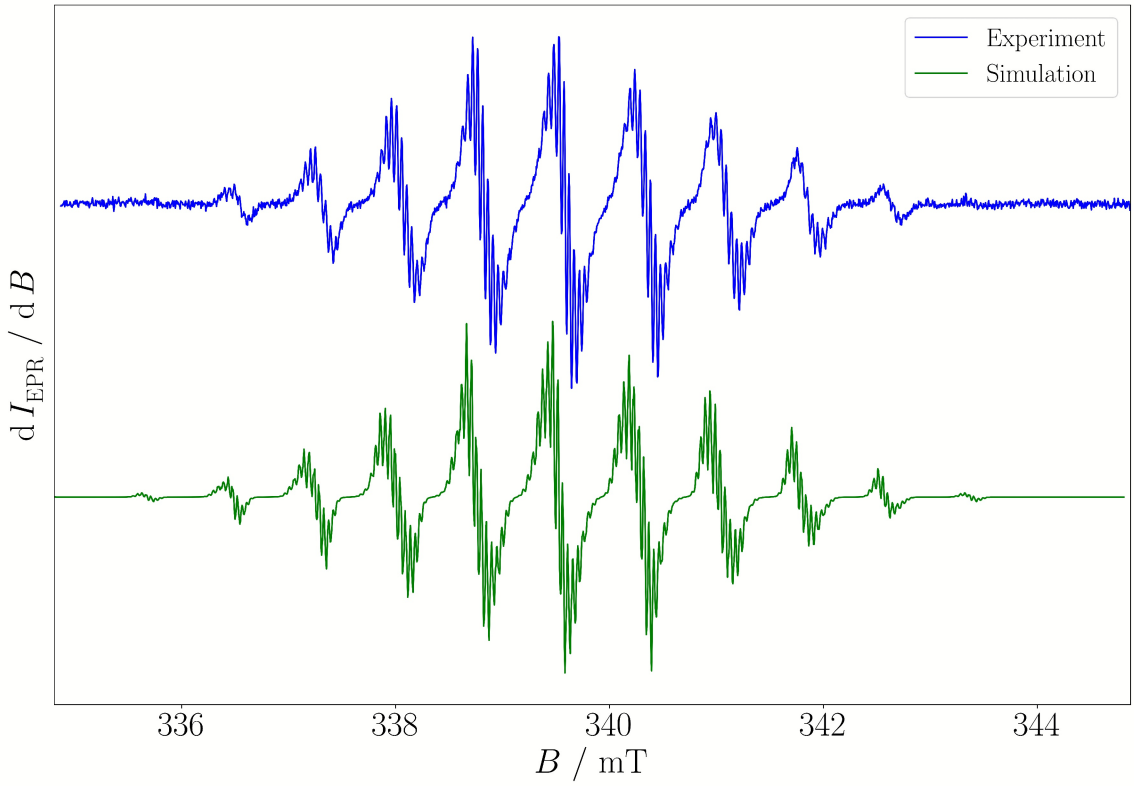

Figure 2. Experimental and simulated EPR spectrum of $\mathbf{1}^{\bullet+}$(Table 1). From potentiostatic electrolysis of 1×10^{-4} M **1** in 0.25 M $TBAPF_6$/DMSO at the first oxidation potential.

Table 1. Isotropic hyperfine coupling/splitting constants (A_{iso}/a_{iso}) of $\mathbf{1}^{\bullet+}$, using the numbering shown in Figure 1 (g_{iso} = 2.0041).

Nucleus	$\lvert A^{sim}\rvert$/MHz	A^{DFT}/MHz	$\lvert a^{sim}\rvert$/mT	a^{DFT}/mT
$2 \times {}^{14}N$ (1,3)	19.911	16.489	0.710	0.588
$3 \times {}^{1}H$ [C(14)H_3]	22.700	26.045	0.810	0.929
$3 \times {}^{1}H$ [C(17)H_3]	22.700	26.045	0.810	0.929
$3 \times {}^{1}H$ [C(15)H_3]	1.011	−1.252	0.036	−0.045
$3 \times {}^{1}H$ [C(16)H_3]	1.011	−1.252	0.036	−0.045
$2 \times {}^{1}H$ [C(5)H, C(8)H]	0.055	−0.034	0.002	−0.001
$2 \times {}^{1}H$ [C(6)H, C(7)H]	1.335	−1.025	0.048	−0.037

Radical Anion $\mathbf{1}^{\bullet-}$. Simulation of the EPR spectrum (Figure 3; for an expanded view see Figure S4) yielded the hyperfine coupling/splitting constants shown in Table 2 along with their DFT-calculated values. The constants differ strongly from those found for $\mathbf{1}^{\bullet+}$, especially those for the nitrogen nuclei, which are now an order of magnitude smaller. There are no really close comparisons with literature values that can be made, but those reported[5,6] for radical anions of 1,4-naphthoquinones carrying a single donor substituent in 2-position are similar to the entries found in Table 2. The agreement between the observed and the calculated values is again excellent, and the largest discrepancy is 0.333 MHz/0.012 mT. The structure of $\mathbf{1}^{\bullet-}$, too, can be considered confirmed.

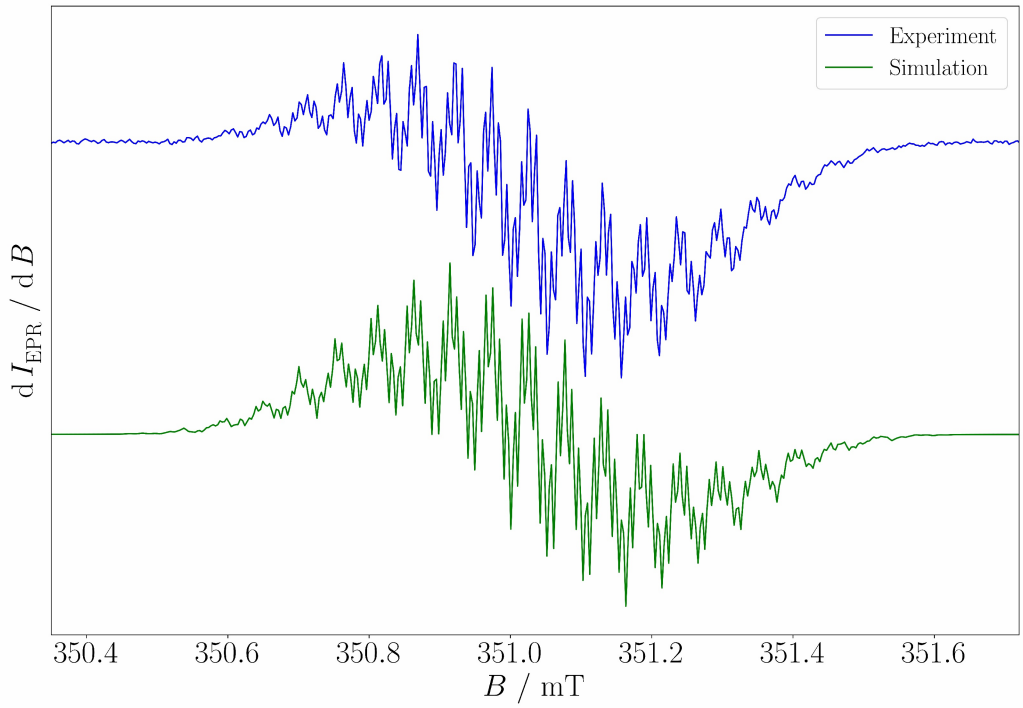

Figure 3. Experimental and simulated EPR spectrum of $\mathbf{1}^{\bullet-}$ (Table 2). From potentiostatic electrolysis of 1×10^{-4} M **1** in 0.25 M $TBAPF_6$/DMSO at the first oxidation potential.

Table 2. Isotropic hyperfine coupling/splitting constants (A_{iso}/a_{iso}) of $\mathbf{1}^{\bullet-}$, using the numbering shown in Figure 1 (g_{iso} = 2.0049).

Nucleus	$\lvert A^{sim}\rvert$/MHz	A^{DFT}/MHz	$\lvert a^{sim}\rvert$/mT	a^{DFT}/mT
$2\times^{14}$N(1,3)	2.695	2.375	0.096	0.085
$3\times^{1}$H [C(14)H_3]	1.577	1.645	0.056	0.059
$3\times^{1}$H [C(17)H_3]	1.577	1.645	0.056	0.059
$3\times^{1}$H [C(15)H_3]	0.047	0.064	0.002	0.002
$3\times^{1}$H [C(16)H_3]	0.524	0.661	0.019	0.024
$2\times^{1}$H [C(5)H, C(8)H]	1.345	−1.012	0.048	−0.036
$2\times^{1}$H [C(6)H, C(7)H]	2.715	−2.698	0.097	−0.096

The calculated total spin density in both radical ions is visualized in Figure 4 and its natural bonding orbital (NBO) analysis is presented in Table 3.

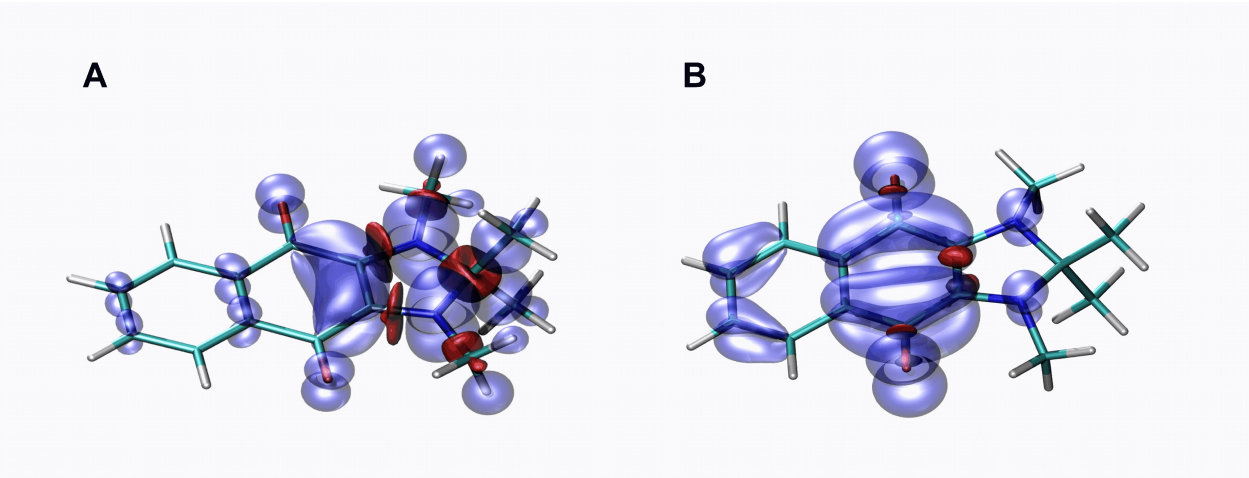

Figure 4. Visualization of B3LYP/EPR-II total spin density (A, radical cation $\mathbf{1}^{\bullet+}$; B, radical anion $\mathbf{1}^{\bullet-}$). Blue (red) surfaces: positive α (negative β) spin density (iso-value, 0.0012 eÅ^{-3}).

Table 3. DFT computed total NBO spin populations for individual atoms and groups, ρ^+ in $\mathbf{1}^{\bullet+}$ and ρ^- in $\mathbf{1}^{\bullet-}$, using the numbering shown in Figure 1.

Atom/Group	ρ^+	ρ^-
N(1)	0.29326	0.02230
N(3)	0.29326	0.02230
C(14)H_3	0.01565	0.00098
C(17)H_3	0.01565	0.00098
C(15)H_3	0.03995	−0.00032
C(16)H_3	0.03995	−0.00119
C_3(4,11,12)O	0.15346	0.43722
C_3(9,10,13)O	0.15346	0.43722
C(5)H	−0.00093	0.00864
C(8)H	−0.00093	0.00864
C(6)H	0.01226	0.03205

C(7)H	0.01226	0.03205

Thermal Stability. We have examined the response of the EPR spectra to sample heating from 323 to 368 K and cooling back in DMSO solution (Figure S6), and to sample cooling from 326 to 253 K and warming back in acetonitrile solution (Figure S7). Both radical ions disappear irreversibly at temperatures above 343 K. Upon cooling, the spectrum of $\mathbf{1}^{\bullet+}$ does not change, but that of $\mathbf{1}^{\bullet-}$ disappears irreversibly. These stability limitations prevented an examination of spectral shape changes that might be associated with a dynamic inversion of the nitrogens in the five-membered ring that flips the methyl groups in 15- and 16-positions between pseudoaxial and pseudoequatorial orientations.

Isotopic Labeling. The inequivalence of the methyl groups in 15- and 16-position in the radical anion $\mathbf{1}^{\bullet-}$ prompted us to verify this result by examination of an analog **2**, labeled with ^{13}C at both of these methyls.

Radical Cation $\mathbf{2}^{\bullet+}$. Observed and simulated EPR spectra of $\mathbf{2}^{\bullet+}$ are shown in Figure 5 and the resulting HF coupling/splitting constants are summarized in Table 4 together with their DFT calculated counterparts. Good agreement between the theory and experiment was found (the largest discrepancy in *A/a* is 3.30 MHz/0.12 mT). Comparison of Figures 1 and 5 and of Tables 1 and 4 highlights the effect of the isotopic replacement and confirms that the methyl groups in 15- and 16-positions are equivalent. It also provides an estimate of the error in the determination of the coupling/splitting constants from the independent spectral fitting for $\mathbf{1}^{\bullet+}$ and $\mathbf{2}^{\bullet+}$, since their values should be essentially identical in both tables (except for C15 and C16, which are absent in Table 1). The values agree within 0.13 MHz (0.005 mT), and the *g* values agree within 0.0001.

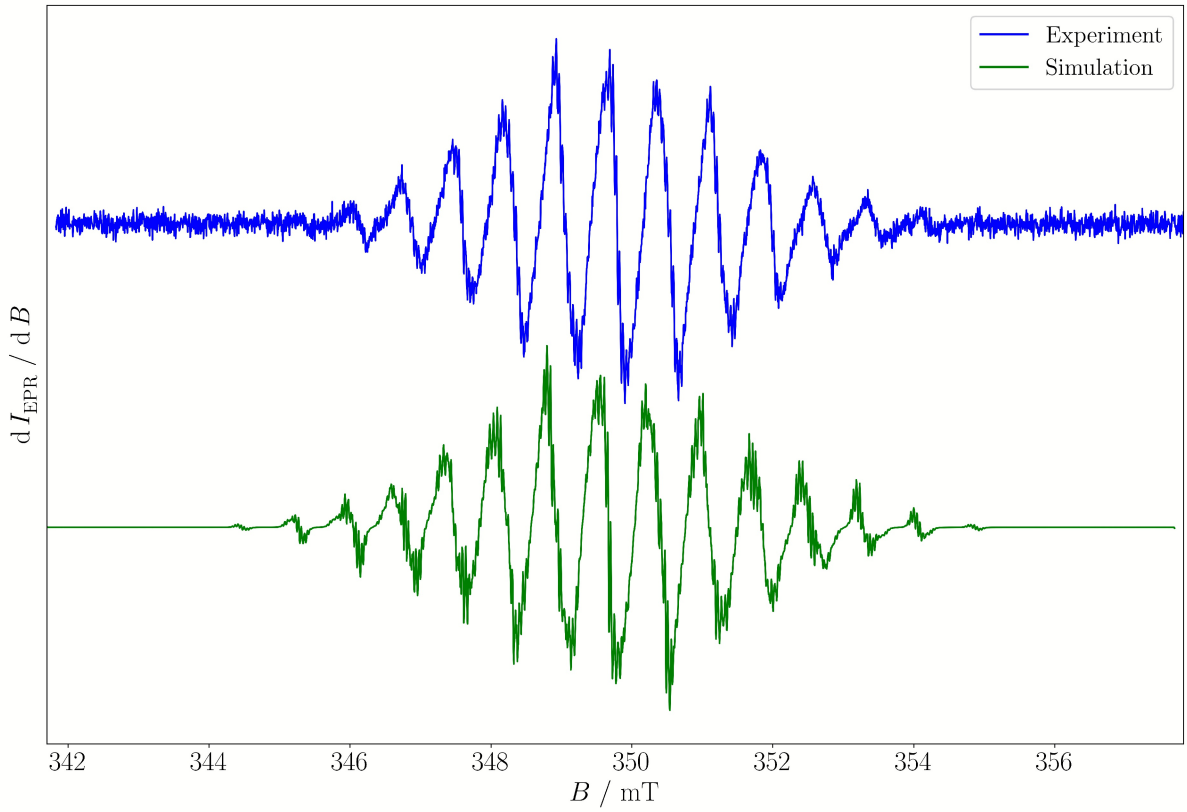

Figure 5. Experimental and simulated EPR spectrum of **2**$^{\bullet+}$(Table 4). From potentiostatic electrolysis of 1 × 10^{-4} M **2** in 0.25 M $TBAPF_6$/DMSO at the first oxidation potential.

Table 4. Isotropic hyperfine coupling/splitting constants (A_{iso}/a_{iso}) of **2**$^{\bullet+}$, using the numbering shown in Figure 1 (g_{iso} = 2.0042).

Nucleus	$\|A^{sim}\|$/MHz	A^{DFT}/MHz	$\|a^{sim}\|$/mT	a^{DFT}/mT
2 × ^{14}N (1,3)	19.796	16.489	0.706	0.588
3 × ^{1}H [C(14)H_3]	22.797	26.045	0.813	0.929
3 × ^{1}H [C(17)H_3]	22.797	26.045	0.813	0.929
2 × ^{13}C(15,16)	37.736	37.473	1.346	1.337
3 × ^{1}H [C(15)H_3]	1.020	−1.252	0.036	−0.045
3 × ^{1}H [C(16)H_3]	1.020	−1.252	0.036	−0.045
2 × ^{1}H [C(5)H, C(8)H]	0.039	−0.034	0.001	−0.001
2 × ^{1}H [C(6)H, C(7)H]	1.467	−1.025	0.052	−0.037

Radical Anion $2^{\bullet-}$. Simulation of the observed unresolved EPR spectrum of $\mathbf{2}^{\bullet-}$ (Figure 6), starting with the constants deduced above for $\mathbf{1}^{\bullet-}$, produced the HF coupling/splitting constants shown in Table 5 along with their DFT calculated values. Good agreement is again apparent (the largest discrepancy in *A/a* is 0.338 MHz/0.012 mT). Comparison with Figure 2 and Table 2 shows once more clear effects of the isotopic replacement and confirms that in this case the methyl groups in 15- and 16-positions are inequivalent. It also provides another estimate of the accuracy of our determination of the coupling/splitting constants from the spectral fitting for $\mathbf{1}^{\bullet-}$ and $\mathbf{2}^{\bullet-}$, which is again seen to be about 0.05 MHz (0.002 mT). The *g* values agree within 0.0001.

The simulation of the EPR spectrum of $\mathbf{2}^{\bullet-}$ was repeated under the constraint of equivalence of the methyl groups in 15- and 16-positions, by assigning average *A/a* values both to the carbon atoms (−1.619 MHz) and to the protons (0.300 MHz). The resulting spectrum differed distinctly from that observed (Figure 6).

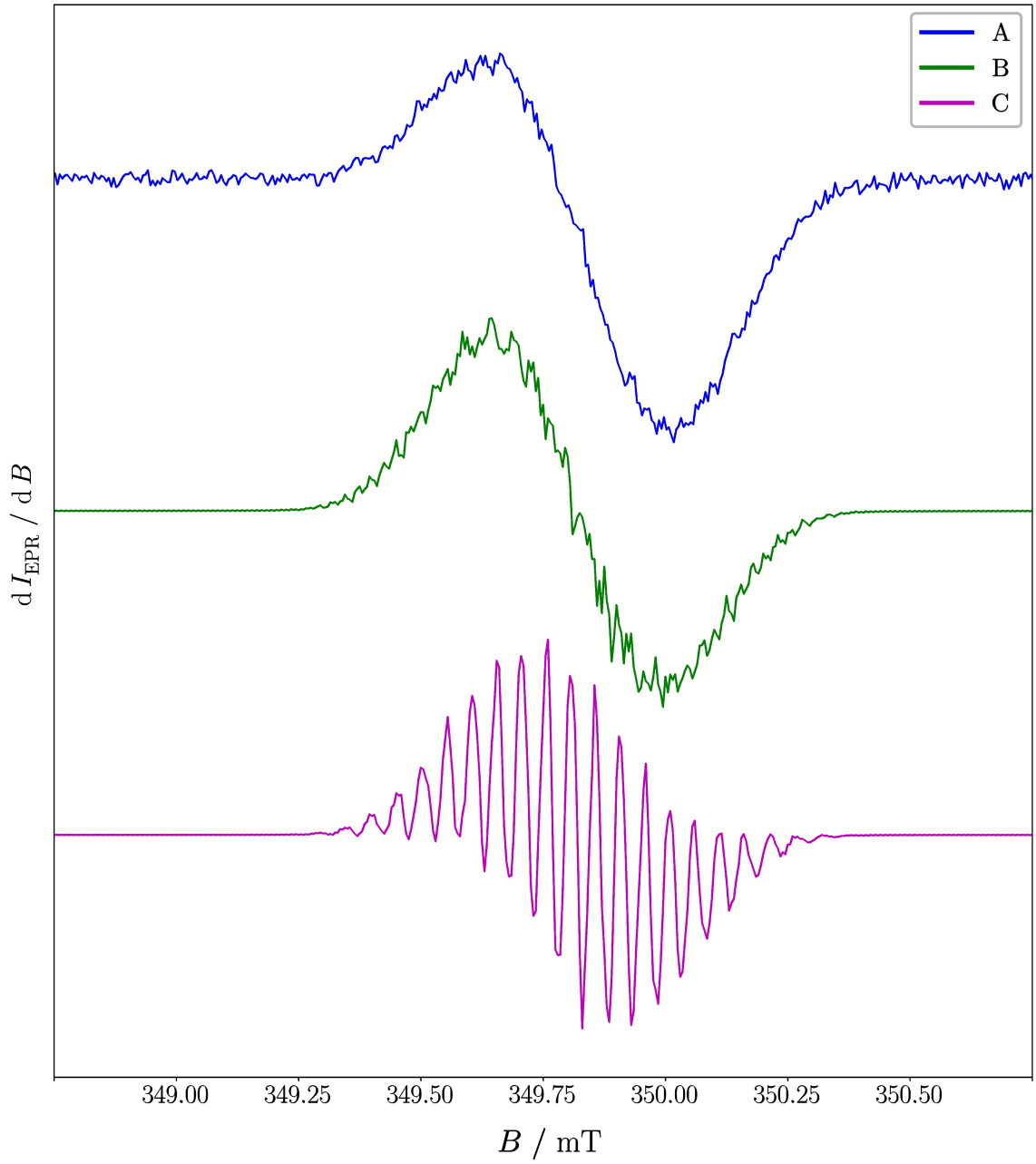

Figure 6. Observed (A) and simulated (B, C) EPR spectra of $\mathbf{2}^{\bullet-}$ (Table 5). The methyl groups $^{13}C(15)H_3$ and $^{13}C(16)H_3$ were either allowed to be inequivalent (B) or forced to be equivalent (C). From potentiostatic electrolysis of 1×10^{-4} M **2** in 0.25 M $TBAPF_6$/DMSO at the first oxidation potential.

Table 5. Isotropic hyperfine coupling/splitting constants (A_{iso}/a_{iso}) of $\mathbf{2}^{\bullet-}$, using the numbering shown in Figure 1 (g_{iso} = 2.0048).

Nucleus	$\lvert A^{sim}\rvert$/MHz	A^{DFT}/MHz	$\lvert a^{sim}\rvert$/mT	a^{DFT}/mT
2 × ^{14}N (1,3)	2.676	2.375	0.095	0.085
3 × ^{1}H [C(14)H$_3$]	1.585	1.645	0.057	0.059
3 × ^{1}H [C(17)H$_3$]	1.585	1.645	0.057	0.059
1 × ^{13}C(15)	2.362	−2.323	0.084	−0.083
1 × ^{13}C(16)	0.875	−0.805	0.031	−0.029
3 × ^{1}H [C(15)H$_3$]	0.045	0.064	0.002	0.002
3 × ^{1}H [C(16)H$_3$]	0.555	0.661	0.020	0.024
2 × ^{1}H [C(5)H, C(8)H]	1.350	−1.012	0.048	−0.036
2 × ^{1}H [C(6)H, C(7)H]	2.800	−2.698	0.100	−0.096

Discussion

The captodative structure **1** represents an interesting example of a strong π donor fused to a strong π acceptor. This is brought into focus by inspection of the spin density in its radical ions $\mathbf{1}^{\bullet+}$ and $\mathbf{1}^{\bullet-}$ (Figure 4 and Table 3), which can be thought of as mapping out the HOMO and the LUMO of **1**, respectively. The former is located on the amino nitrogens of the five-membered ring and the adjacent carbons and the latter is located on the quinoidal ring.

The basic molecular structure of the radical ions $\mathbf{1}^{\bullet+}$ and $\mathbf{1}^{\bullet-}$ has been confirmed beyond doubt and the only structural issue that can be debated is the planarity of the five-membered ring, coupled with a pyramidalization at its two nitrogen atoms. The single-crystal X-ray structure of neutral **1** shows a slight but distinct degree of pyramidalization on the nitrogen atoms,[9] and hence a double minimum, where the two forms differ in the sense of this pyramidalization. The EPR spectrum of $\mathbf{1}^{\bullet+}$ would be compatible with a very shallow double minimum in the ground state potential energy surface and a pair of very rapidly interconverting structures, but there is no reason to question the

DFT result for this radical cation that predicts a single minimum with a planar five-membered ring. Although the natural tendency of the amino substituent is to pyramidalize as in ammonia, in compounds such as $\mathbf{1}^{\bullet+}$, in which the amino group is positively charged and conjugated with a strong π electron acceptor, this tendency is overruled and the amino nitrogen atoms become planar.

In $\mathbf{1}^{\bullet-}$, the extra electron present mostly in the quinoidal ring suppresses its π-electron withdrawing tendency, the amino nitrogens revert to their natural pyramidal structure, and a double minimum with a puckered five-membered ring results, making one of the two methyl groups carried by ring carbon axial and the other equatorial, hence inequivalent. This has been convincingly proven by examination of the effects of isotopic substitution, a well established tool.[10,11] Our attempt to determine the rate of interconversion between the two structures and the height of the barrier separating the two minima was however thwarted by the limited thermal stability of $\mathbf{1}^{\bullet-}$. The calculated barrier height is 1.9 kcal/mol.

It is noteworthy that the radical anion $\mathbf{1}^{\bullet-}$ is destroyed not only by heating, but also by cooling. It is likely that there is an easy reaction path from its dimer to closed-shell products that makes the dimerization irreversible, but we did not investigate it.

Experimental Part

Materials. 1,2,2,3-Tetramethyl-2,3-dihydro-1H-naphtho[2,3-d]imidazole-4,9-dione (**1**) was synthesized and purified as reported.[8] Compound **2** was prepared by the same method, except that $(^{13}CH_3)_2CO$ was used instead of $(CH_3)_2CO$ in the last step. ^{1}H NMR (300 MHz, C_6D_6): δ 8.00 (dd, J = 3.3 Hz and 5.6 Hz, 2H, -C-C*H*-CH-), 6.97 (dd, J = 3.3 Hz and 5.6 Hz, 2H, -C-CH-C*H*-), 2.88 (s, 6H, N-CH_3), 0.77 (d, J = 129.9 Hz, 6H, -C-CH_3); ^{13}C NMR (75 MHz, C_6D_6): δ 176.2, 133.2,

133.1, 132.0, 124.5, 87.0, 29.2, 20.5.

Anhydrous acetonitrile (CH_3CN) and dimethylsulfoxide (DMSO), with water content below 0.001%, were purchased from Sigma-Aldrich and stored over molecular sieves activated at 473 K. Tetrabutylammonium hexafluorophosphate ($TBAPF_6$, ≥ 99.0%, puriss., for electrochemical analysis) was purchased from Sigma-Aldrich as well and used as electrolyte. Prior to experiments it was dried under reduced pressure at 353 K for 3 h.

EPR Spectroscopy and Spectroelectrochemistry. EPR spectra were recorded with a Bruker EMX^{plus} 10/12 CW (continuous wave) EPR spectrometer equipped with a Premium-X-band microwave bridge. The g_{iso} factor of the radical cation/anion was determined using a built-in spectrometer frequency counter and a ER-036TM NMR-Teslameter. A flat EPR quartz cell (Bruker ER160FCQ) was used for room-temperature EPR spectroelectrochemical experiments. A home-built three-electrode system consisting of a Pt wire contacted with Pt μ-mesh (working electrode), an Ag wire (quasi-reference electrode), and a Pt wire (counter electrode), was inserted into the EPR cell and finally into the Bruker ER4102ST EPR cavity. For the radical anion, also the high sensitivity Bruker ER4119HS EPR cavity was used to obtain optimally resolved spectra. Inactive electrode parts were isolated either with a teflon tape or sealed in a glass capillary. After each EPR spectroelectrochemical measurement the stability of the Ag quasi-reference electrode was checked against the ferrocene/ferricenium ($Fc^{0/+1}$) couple. Prior to each measurement, a solution of **1** or **2** in 0.25 M $TBAPF_6/CH_3CN$ or in 0.25 M $TBAPF_6$/DMSO was thoroughly flushed with nitrogen to minimize the influence of atmospheric oxygen on the electrochemical experiments and on the EPR line broadening. Simultaneous voltammetric and potentiostatic experiments were controlled by a Potentiostat/Galvanostat Autolab PGSTAT302N (Metrohm). The experiments at higher (up to 368

K) and lower (down to 253 K) temperatures were controlled by a liquid/gas nitrogen unit ER 4141VT-U and the Win-EPR acquisition software (both from Bruker). During variable-temperature measurements a compatible EPR flat cell (ER165FCVTQ, Bruker) with a 3-electrode system was used. Therefore the resonance condition (microwave frequency and the corresponding magnetic flux density) for an identical sample differs.

Computations. Simulations of the EPR spectra were performed with a MATLAB toolbox EasySpin program (v. 5.1.10) by least-squares fitting to an experimental spectrum using a combination of Nelder-Mead simplex and Particle swarm algorithms.[12] Instrumental parameters such as microwave frequency, central field, sweep width, number of points, and modulation amplitude were included in the simulation. The simulations assumed fast rotation for the $–CH_3$ groups, averaging the hyperfine (HF) splitting/coupling constant for their three protons. This is reasonable, given that the EPR spectra were recorded in solution at temperatures ranging from 253 to 368 K. The number of digits reported in the tables below for the constants *A* and *a* corresponds to the number actually used in producing the simulated spectra shown in the figures below and is larger than the number of digits that are significant. Comparison of the results for **1** and **2** suggests that the accuracy of the determination is 0.01 - 0.13 MHz for *A* and 0.0003 - 0.004 mT for *a*.

All DFT computations were performed with the Gaussian 09 quantum chemical package (version D.01).[13] The geometry of radical ions was optimized at the B3LYP/6–311G(d,p) level and the EPR parameters such as *g* factor and hyperfine splitting/coupling constants were calculated by the B3LYP/EPR–II method[14] using the conducting polarizable continuum model (C-PCM)[15] for both solvents (CH_3CN and DMSO). The computations assumed that the rotation of the methyl groups is fast and the computed hyperfine (HF) splitting/coupling constant for their three protons were

averaged. Energy barrier for the fast exchange of methyl groups –C(15)H_3 and –C(16)H_3 was calculated by the synchronous transit-guided quasi-Newton (STQN) method[16] with the QST3 option implemented in Gaussian. Molecular structures as well as spin densities were visualized by the Visual Molecular Dynamics (VMD)[17] and/or by PyMol[18] software packages.

Acknowledgment. This material is based upon work supported by the U.S. Department of Energy, Office of Science, Office of Basic Energy Sciences (DE-SC0007004), the Grant Agency of the Czech Republic (GA15-19143S), and the Institute of Organic Chemistry and Biochemistry, Academy of Sciences of the Czech Republic (RVO: 61388963).

Supporting Information. Cyclic voltammograms of **1** and **2**, temperature (for $\mathbf{1}^{\bullet-}$, also solvent) dependence of EPR spectra of $\mathbf{1}^{\bullet+}$ and $\mathbf{1}^{\bullet-}$, and spectra obtained after potentiostatic electrolysis followed by disconnection from the electrodes. ^{1}H and ^{13}C NMR spectra of **2**. DFT optimized geometries of $\mathbf{1}^{\bullet+}$ and $\mathbf{1}^{\bullet-}$. Expanded observed and simulated EPR spectra of $\mathbf{1}^{\bullet-}$. Complete reference 10.

References

[1] Wen, J.; Havlas, Z.; Michl, J. Captodatively Stabilized Biradicaloids as Chromophores for Singlet Fission. *J. Am. Chem. Soc.* **2014**, *137*, 165–172.

[2] Smith, M. B.; Michl, J. Singlet Fission. *Chem. Rev.* **2010**, *110*, 6891–6936.

[3] Dexter, D. L. Two Ideas on Energy Transfer Phenomena: Ion-Pair Effects Involving the OH Stretching Mode, and Sensitization of Photovoltaic Cells. *J. Lumin.* **1979**, *18*, 779–784.

[4] Hanna, M. C.; Nozik, A. J. Solar Conversion Efficiency of Photovoltaic and Photoelectrolysis Cells with Carrier Multiplication Absorbers. *J. Appl. Phys.* **2006**, *100*, 074510.

[5] Hewgill, F. R.; Höffer, U.; Power, R. C.; Stegmann, H. B. ESR Spectra of Some Amino Acid Derivatives of Semiquinone Anions. *Magn. Reson. Chem.* **1996**, 34, 47-51.

[6] Temtsin-Krayz, G.; Shames, A. I.; Bittner, S. Radical Decomposition of N,N-bis-(3-chloro-1,4-naphthoquinon-2-yl) Amine in Basic Conditions followed by EPR. *Res. Chem. Intermed.* **2003**, *29*, 325-333.

[7] Eltsov, A. V.; Kuznetsov, V. S. 1,2-Dihydrobenzimidazole Derivatives. *Zh. Org. Khimii* **1966**, *2*, 1482-1489.

[8] Dron, P. I.; Ramešová, Šárka; Holloran, N. P.; Pospíšil, L.; Michl, J. Redox Behavior of 2,3-Diamino-1,4-Naphthoquinone and Its N -Alkylated Derivatives. *Electroanalysis* **2016**, *28*, 2855–2860.

[9] Johnson, J. C.; Dron, P. I.; Fatur, S. M.; Michl, J. Solid-State Photophysics of an *N*-Alkylated 2,3-Diamino-1,4-naphthoquinone, unpublished results.

[10] Gerson, F.; Huber, W. Electron Spin Resonance Spectroscopy of Organic Radicals; Wiley-VCH Verlag GmbH & Co. KGaA, 2003.

[11] Kaleta, J.; Tarábek, J.; Akdag, A.; Pohl, R.; Michl, J. The 16 $CB_{11}(CH_3)_n(CD_3)_{(12-n)}$ Radicals with 5-Fold Substitution Symmetry: Spin Density Distribution in $CB_{11}Me_{12}$. *Inorg. Chem.* **2012**, *51*, 10819–10824.

[12] Stoll, S.; Schweiger, A. EasySpin a Comprehensive Software Package for Spectral Simulation and Analysis in EPR. *J. Magn. Reson.* **2006**, *178*, 42–55.

[13] Gaussian 09, Revision D.01, Frisch, M. J.; et al. Gaussian, Inc., Wallingford CT, 2009.

[14] Barone, V. Recent Advances in Density Functional Methods:(Part I); Chong, D. P., Ed.; World Scientific, 1995; Vol. 1.

[15] Barone, V.; Cossi, M. Quantum Calculation of Molecular Energies and Energy Gradients in Solution by a Conductor Solvent Model. *J. Phys. Chem. A* **1998**, *102*, 1995–2001.

[16] Cossi, M.; Rega, N.; Scalmani, G.; Barone, V. Energies Structures, and Electronic Properties of Molecules in Solution with the C-PCM Solvation Model. *J. Comp. Chem.* **2003**, *24*, 669–681.

[17] Humphrey, W.; Dalke, A.; Schulten, K. VMD – Visual Molecular Dynamics. *J. Mol. Graphics* **1996**, *14*, 33–38.

[18] Schrödinger, L. L. C. The PyMOL Molecular Graphics System, Version 1.8, 2015.